Post-migration image optimization of multi-azimuth legacy data in Central Santos Basin

Hongyan Li, Pedro Barro, Zhao Ge, Oscar Pérez, Teddy L. Standley, Carina Lansky, and Marcela Ortin, Schlumberger

Copyright 2021, SBGf - Sociedade Brasileira de Geofísica

This paper was prepared for presentation during the 17th International Congress of the Brazilian Geophysical Society held in Rio de Janeiro, Brazil, 16-19 August 2021.

Contents of this paper were reviewed by the Technical Committee of the 17th International Congress of the Brazilian Geophysical Society and do not necessarily represent any position of the SBGf, its officers or members. Electronic reproduction or storage of any part of this paper for commercial purposes without the written consent of the Brazilian Geophysical Society is prohibited.

Abstract

In complex presalt reservoirs such as the Santos Basin in Brazil, improvements in our techniques for combining and imaging legacy datasets can postpone the need for additional costly seismic acquisitions. In this case study, we show how data from several legacy acquisitions with varying azimuths were carefully combined to create a contiguous multi-azimuth image. Two different migration algorithms are used with each having tailored approaches for the weighting and summation of the migrated data. Compared to the legacy image, significant improvement is attained in terms of signal-to-noise ratio, the coherency of evaporite layers, base salt, presalt, and basement events, and the delineation of the pre-salt faults.

Introduction

In 2006, the giant presalt field Lula was discovered in Santos Basin. At that time, the only available seismic data in the area were 2D lines and narrow-azimuth (NAZ) streamer data. Today, with Santos Basin being one of the world's most promising exploration and production areas, rigorous seismic imaging is required to better understand the producing fields and to facilitate the development of other prospects. By combining the data from several previous seismic acquisitions in this area, we can generate multi-azimuth (MAZ) data to produce high-resolution imaging in the central Santos area (Ortin et al., 2020).

In the study area, three NAZ streamer datasets are available, each being acquired with a different shooting direction (HD4D, 123.6º; Franco, 158º; Constellation, 90º) between 2002 and 2012. Additionally, part of this area is covered by Iara, a full-azimuth data acquired in 2011 with a circular shooting technique (Figure 1). HD4D is the largest survey, covering most of the study area. Reverse time migration (RTM) and Kirchhoff depth migration (KDM) are both used to generate the final imaging products. This paper will showcase the different techniques used to combine these legacy datasets to form the MAZ RTM and KDM images separately.

Data Preparation for Imaging

To ensure that all four datasets combine seamlessly, the four legacy datasets were re-datumed to mean sea level during adaptive deghosting (Rickett, 2014; Zarkhidze, et al., 2016) and was followed by water velocity correction (Carvill, 2009) and survey matching. Following this, the combined legacy data were used together for surface multiple prediction (Dragoset et al., 2010) to increase crossline aperture, and therefore improving the surface-multiple modeling and elimination. The combined legacy data, with the varying azimuths, were then input to full-waveform inversion (FWI; Vigh and Starr, 2008) followed by multi-scale, multi-azimuth, common image point (CIP) Tomography (Woodward et al., 2008) improving the velocity model accuracy, reducing the uncertainty of the model and suppressing the acquisition footprint. In order to create the optimum high-resolution image, the legacy data were migrated separately and then summed together based on seismic semblance coherency.

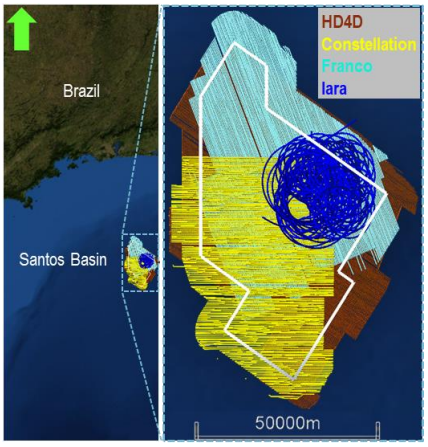

Figure 1 *- Central Santos MAZ Reimaging project area and input surveys shot maps. HD4D, Constellation, and Franco are NAZ surveys, and Iara is full-azimuth survey acquired with a circular shooting technique.*

Coherency-based weighted summation

For coherency-based weighted summation, the semblance analysis volume (SAV) is calculated as:

$$S_{D,X,Y} = \frac{\sum_d \left[\sum_{x,y} w_{x,y} f_{d,x,y} \Big/ \sum_{x,y} w_{x,y}\right]^2}{\sum_d \sum_{x,y} w_{x,y} f_{d,x,y}^2 \Big/ \sum_{x,y} w_{x,y}}$$

Where $S_{D,X,Y}$ is the weighted normalized semblance coefficient for a specific depth D and spatial location X,Y. The result is the energy of the summed data normalized by the mean energy of the data. Each semblance coefficient $S_{D,X,Y}$ is evaluated for a depth window centered at depth D and a rectangular spatial window centered at location X,Y. Spatially-variant weights w may be specified. Semblance coefficients range from zero to one, with one representing spatial continuity (i.e., all traces are identical). For each

survey, a polygon was defined based on the full-fold coverage of the survey. The coherency based weighted summation is derived as:

Weighted summation = $\sum Si*Pi*Ki*Di/\sum Si*Pi$

Where Di is the seismic image from i^{th} survey; Si is the semblance coherency volume from i^{th} survey, ranging from 0 to 1; Pi is the full fold coverage of i^{th} survey, ranging from 0 to 1. Ki is the scalar to match the amplitude of different surveys to the same level. Even matching the seismic trace amplitude to the same level before migration, the RTM migration amplitude is different due to the different data configuration.

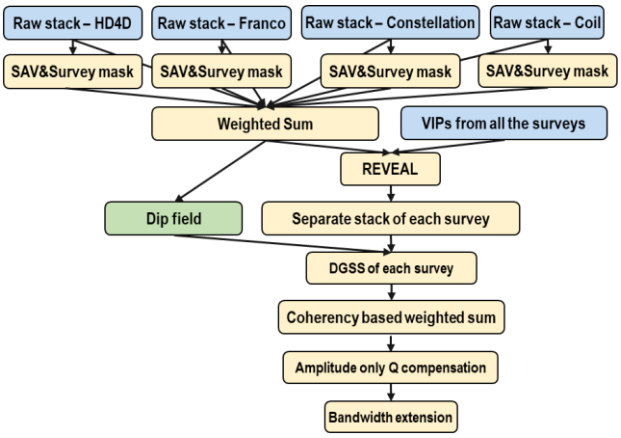

Figure 2 *- RTM post-processing flow. SAV – semblance analysis volume; VIPs – vector image partitions; REVEAL – residual event alignment; DGSS – dip guided selective stack.*

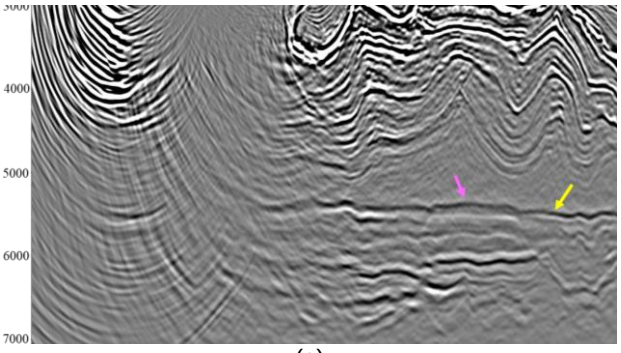

(a)

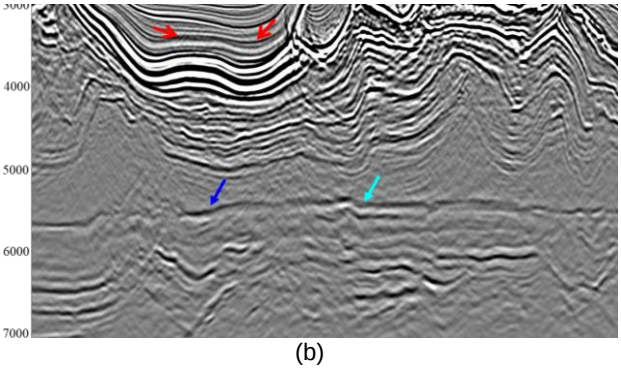

(b)

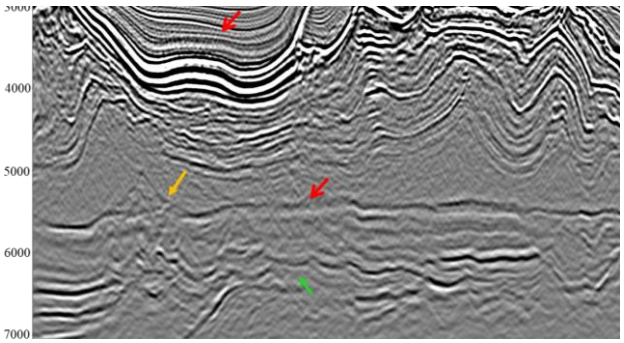

(c)

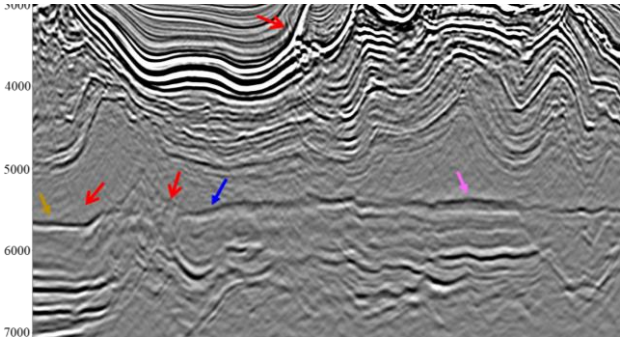

(d)

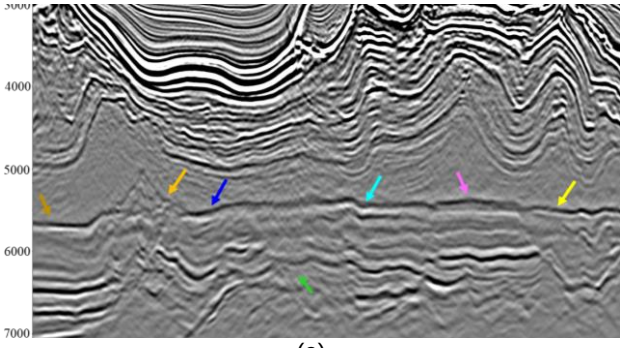

(e)

Figure 3 *- Raw RTM image from individual surveys and the coherency-based weighted summation. (a) Iara; (b) Franco; (c) Constellation; (d) HD4D; (e) Weighted summation of (a)-(d). Red arrows point to migration swings observed in each survey. In the merged image (e), the base salt indicated by the yellow arrow is mainly contributed to by (a) Iara, the pink arrow area is mainly contributed to by (a) Iara and (d) HD4D; the cyan arrow area is mainly contributed to by (b) Franco; the blue arrow area is mainly contributed to by (b) Franco and (d) HD4D; the orange arrow area is mainly contributed to by (c) Constellation; the brown arrow area is mainly contributed by (d) HD4D. The presalt area indicated by the green arrow is mainly contributed by (c) Constellation.*

RTM image Enhancement

For RTM migration, 45 Hz vector image partitions (VIPs) were output with minimum additional cost for image enhancement (Zhao et al., 2015). The RTM post-processing flow is shown in Figure 2. Residual event alignment was applied to these RTM VIPs to improve seismic coherency. Seismic semblance was calculated for

the stacks of each individual survey, and a weighted summation was then carried out based on the semblance coherency. 3D dip decomposition (Nichols et al., 2017) and dip-guided selective stack (DGSS) (Gu et al., 2018) were applied to the RTM image to suppress migration swings that have different dips compared to the full image to improve seismic coherency. The DGSS was applied only inside salt and presalt regions, with milder parameters in the presalt zone to avoid attenuation of the abundant faults. Amplitude-only Q compensation and bandwidth extension were applied to the RTM to further enhance the resolution.

Figure 3(a)-3(d) are the individual raw RTM images from the four legacy surveys after amplitude scaling. Figure 3(e) is the weight-summed image. Many of the swings observed in the individual surveys (Red arrows) disappear after weighted summation. Also, the base salt and presalt horizons become much more coherent and continuous on the merged image. The arrows indicate the different surveys contributing to various parts of the merged image.

The application of the DGSS was designed to further refine the image post summation to reduce the operator energy which conflicts with the geological dip as shown in Figure 4. The orange arrows point to regions where the DGSS application reduced the operator energy within both the salt and the presalt regions.

In summary, by migrating the MAZ data separately and output VIPs, optimum RTM image enhancement was achieved by residual event alignment of the VIPs, DGSS of individual survey stacks, and semblance coherency based weighted summation of all the DGSS outputs from individual surveys.

KDM Image Enhancement

For the KDM, we output 90 Hz surface offset gathers and modified the enhancement flow accordingly (Figure 5). On these KDM gathers, strong interbed and/or converted waves were observed due to the high-velocity carbonate and salt layers, hence high-resolution Radon (Moore and Kostov, 2002) was applied to attenuate residual multiples, converted waves, and interbed multiples. Curvelet domain subtraction (Yu and Yan, 2011) was applied to the Radon noise model to avoid signal leakage from the Radon transform at the near offsets. Residual event alignment was applied to the KDM gathers to improve seismic coherency, and structural smoothing (Hale, 2011) was applied to the KDM image to attenuate high-frequency noise.

Figure 6 shows the raw KDM gathers (6a), after high-resolution Radon and Curvelet transform (6b), and the difference between the two (6c). The signal coherency is improved after this process without observed signal leakage. In Figure 6, the annotation of 1, 2, and 3 represent HD4D, Franco, and Constellation KDM gathers separately.

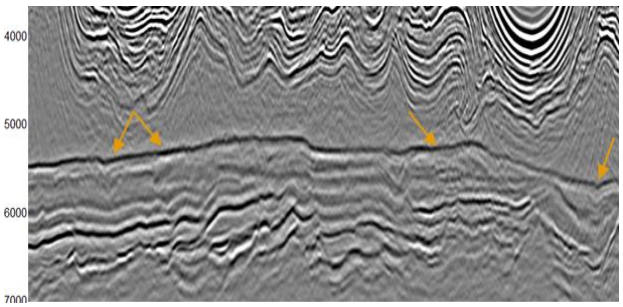

(a)

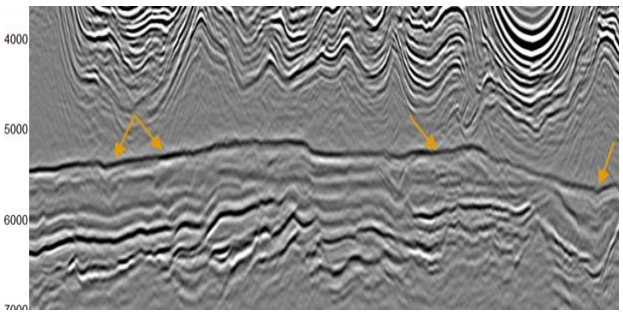

(b)

***Figure 4** - Weight summed RTM image before (a) and after (b) DGSS to attenuate migration swings inside the salt and in the presalt.*

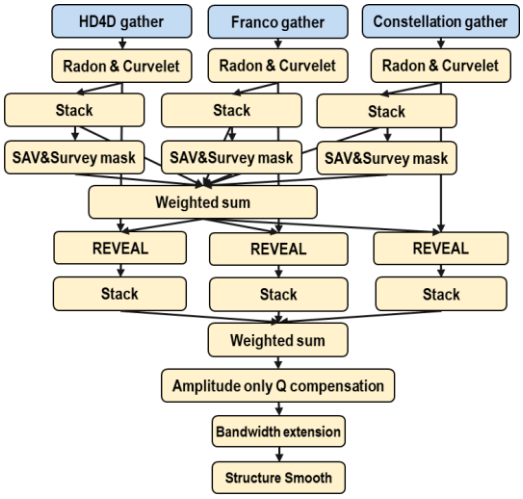

***Figure 5** - KDM post-processing flow.*

Comparing KDM with RTM image, more high-frequency noise is observed on KDM image after Q compensation and bandwidth extension since the maximum frequency is 90 Hz for KDM while 45 Hz for RTM. Structure smoothing is applied to attenuate the high-frequency noise. Figure 7 compares the final processed KDM image before (7a) and after (7b) structure smoothing. It is obvious that some high frequency migration noise (ex., pointed by the yellow arrows) is reduced after structure smoothing without smearing the faults; therefore, the presalt event coherency is improved by mitigating this high frequency migration noise.

In summary, optimum KDM image enhancement was achieved by high-resolution Radon with additional signal protection on KDM gathers to remove residual surface multiples, interbed multiples, and converted waves, residual event alignment to flatten gathers, and semblance coherency based weighted summation of all the individual survey stacks, followed by structure smoothing to attenuate high-frequency noise.

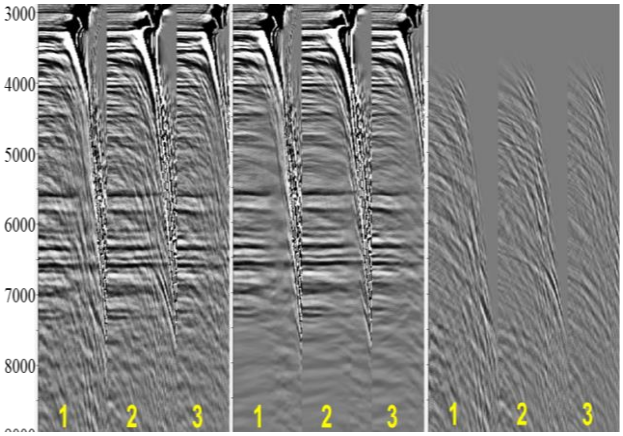

(a) *(b)* *(c)*

Figure 6 *- one KDM gather from 3 NAZ data set. (a) raw gather; (b) after Radon combined with Curvelet transform; (c) the difference of (a) and (b). From left to right, HD4D, Franco and Constellation.*

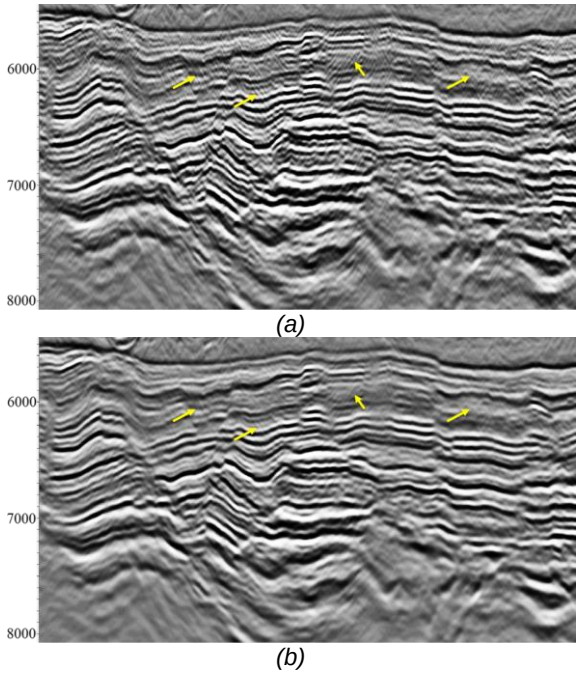

(a)

(b)

Figure 7 *- KDM final enhanced image before (a) and after (b) structure smoothing using the dip field calculated using the final enhanced RTM volume.*

Results

Figure 8 compares the legacy final enhanced KDM image from HD4D data (a), the reprocessed raw KDM image from HD4D data (b), the final enhanced KDM image from the three NAZ surveys (c), the reprocessed raw RTM image from HD4D data (d), and the final enhanced RTM image from all the four surveys (e, three NAZ and one FAZ). With a more accurate post salt velocity model and the improved low frequencies from broadband processing, the pure salt top (Blue arrows) is clearly defined on all the reprocessed images, which is difficult to interpret on the legacy one. Strong migration swings are observed around the base salt and in the presalt zone from the legacy KDM image, which we suggest is due to a combination of the less accurate velocity model, noise in the seismic data, and the limitation of illumination by the NAZ geometry. With a more accurate velocity model from depth processing, improved signal-to-noise ratio (SNR) contributed by improved signal processing, the migration noise is highly reduced in the HD4D reprocessed raw KDM (Figure 8b) and RTM (Figure 8d) image. Comparing with the legacy KDM image (Figure a), the triangle pull-up structure (Green arrow) is clearly defined on the reprocessed raw KDM image (Figure b), which is close to a well location; significant improvement is observed in most areas, although some portions of the base salt amplitude is still weak, and some migration swings are still present. After combining the other two NAZ surveys and with further enhancement, the migration swings in the raw HD4D KDM image are very well suppressed (ex., Cyan arrow in Figure 8b, 8c), the continuity and resolution of base salt and presalt layers are further improved. The weak base salt amplitude in the HD4D raw KDM image (Orange arrows in Figure 8b) is also quite weak in the raw HD4D RTM image (Orange arrows in Figure 8d). After combining the other three surveys and with further enhancement, the weak amplitude becomes much stronger (Orange arrows in Figure 8e). Comparing the enhanced KDM (Figure 8c) and RTM image (Figure 8e), the enhanced RTM image shows better base salt continuity, less high-frequency noise, and more clearly defined presalt events, although lower in resolution with a limited bandwidth (90 Hz KDM vs. 45 Hz RTM). Therefore, the final KDM and RTM products complement each other.

Figures 9 compares the RMS amplitude along base salt from legacy KDM image (a), final enhanced KDM image (b), raw RTM image from HD4D data (c), and the final enhanced RTM image (d). The purple color represents very weak base salt amplitude, which indicates complicated post salt and salt structures. Compared to the legacy image, the base salt RMS amplitude is highly improved on the final enhanced KDM image, but weak amplitude areas are still observed (Pointed by arrows). Comparing Figure 9b and 9c, the raw RTM image shows stronger base salt amplitude than the enhanced KDM image, which demonstrates the advantage of RTM algorithm. The RMS amplitude is further improved in Figure 9d after combining RTM image from the other surveys and further enhancement effort. Significant improvement is observed comparing the legacy KDM and the final RTM RMS amplitude.

In comparing the results from RTM and KDM approaches, we have demonstrated that both benefit from broadband data with a higher SNR, a more accurate velocity model, and the optimized combination of all the images from

different azimuths. However, each algorithm required different enhancement flows to create the optimized final MAZ image. Compared to the legacy imaging, the MAZ reprocessing has achieved a substantial improvement by revisiting all components of the entire workflow. Both showcase the improvements in the SNR with significantly improved base salt and presalt imaging and sharper resolution. In both, the acquisition footprint and migration swings are expressively minimized, and the presalt fault blocks and basement are clearly defined in most places. Therefore, the imaging uncertainty is extremely reduced in both algorithm outputs.

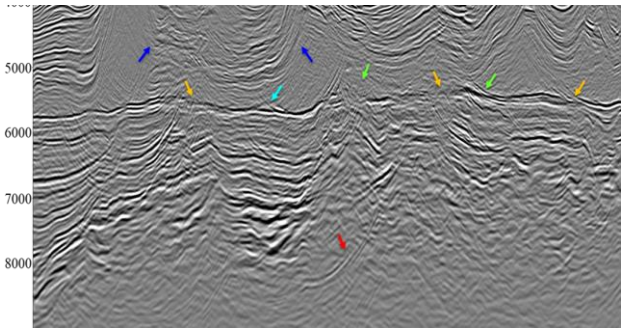

(a)

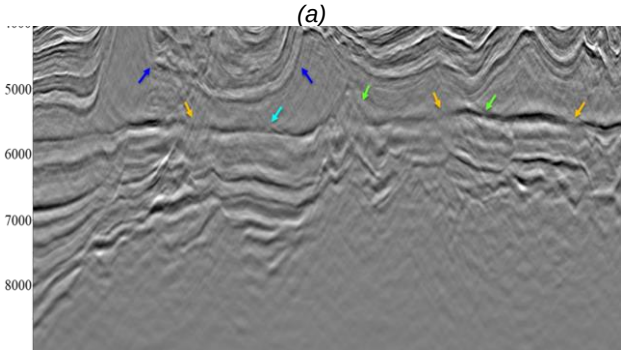

(b)

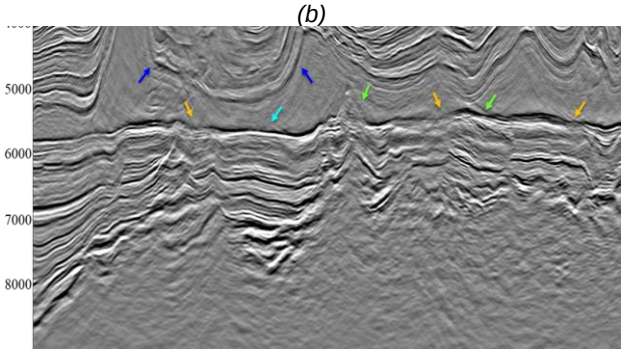

(c)

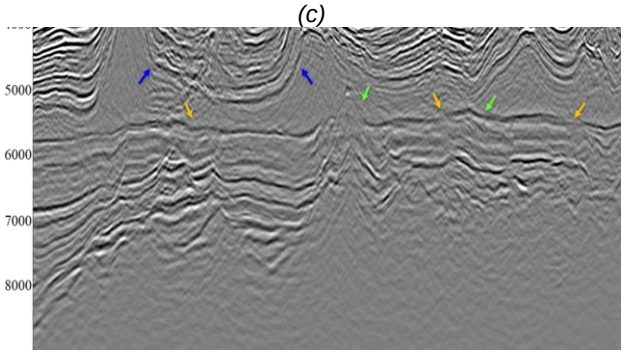

(d)

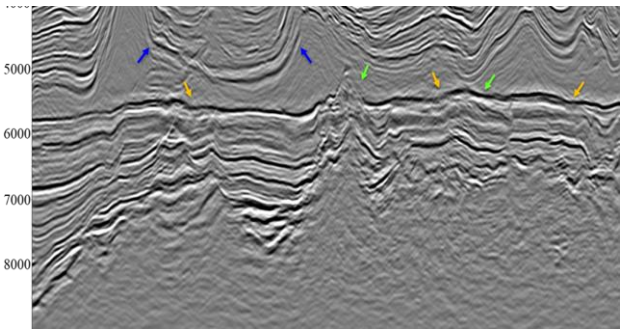

(e)

Figure 8 *- (a) Legacy final enhanced KDM image from HD4D data; (b) Reprocessed KDM raw image from HD4D data; (c) Reprocessed final enhanced KDM image - weighted summation from 3 NAZ surveys; (d) Reprocessed RTM raw image from HD4D data; (e) Reprocessed final enhanced RTM image - weighted summation from 4 surveys. Red arrow in (a) points to migration swing caused by residual surface multiples from legacy data. Blue arrows point to the top of the pure salt; Green arrows point to the base salt that is poorly imaged on legacy image, but continuous on all reprocessed images. Cyan arrow points to the migration swings that are strong on the legacy image, still present on the KDM raw image, but very well suppressed on the KDM enhanced image. The orange arrows point to the base salt that is poorly imaged on the legacy image, quite weak on the KDM and RTM raw images, becomes more coherent on the KDM enhanced image, and further improved on the RTM enhanced image.*

Conclusions

Optimization of separately migrated MAZ images provided further enhancement of the presalt imaging. The SNR improvement is attained through semblance-based weighted summation of all the images from different surveys, signal-protected high-resolution Radon applied to Kirchhoff offset gathers, residual moveout alignment, dip decomposition and dip-guided selective stack, and structure guided smoothing. The image-enhancement workflow is effective in attenuating migration swings, converted waves, interbed multiples, residual surface multiples and high-frequency noise. The signal coherency from each of the surveys is honored by the weighted summation and at the same time, minimizing the noise from each of the individual survey. The seismic resolution is further improved by amplitude-only Q compensation followed by bandwidth extension. Comparing to the legacy image, a superior high-resolution image is achieved by the reprocessing, combination and reimaging of the various legacy datasets in the central Santos Basin.

Acknowledgment

We thank WesternGeco Multiclient for the permission to use the data and we thank all the people involved in processing the project.

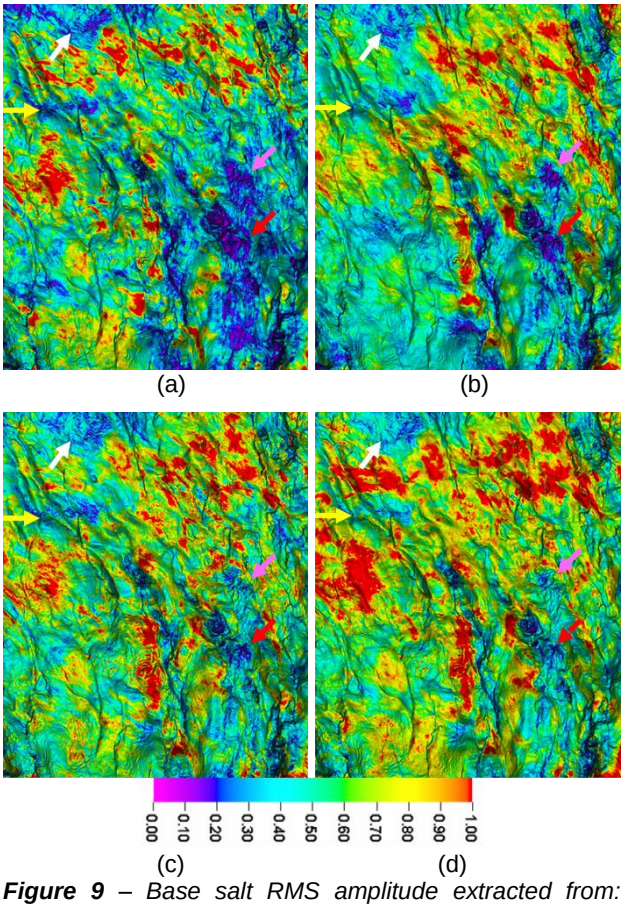

Figure 9 *– Base salt RMS amplitude extracted from: (a) Legacy final enhanced KDM from HD4D data; (b) Reprocessed final enhanced KDM image from MAZ data; (c) Reprocessed raw RTM image from HD4D data; (d) Reprocessed final enhanced RTM image from MAZ data.*

References

Carvill, C.; 2009. A new approach to water velocity estimation and correction. 71st EAGE conference abstracts, Doi: https://doi.org/10.3997/2214-4609.201400384

Dragoset, B.; Verschuur, E.; Moore, I.; and Bisley, R.; 2010, A perspective on 3D surface-related multiple elimination, Geophysics Vol 75, Doi: https://doi.org/10.1190/1.3475413

Espinoza, C.; Sanger, W.; Nicholes, D.; Graniel, J.; 2017. Geology-constrained data-driven multiple prediction, SEG Technical Program Expanded Abstracts, Doi: https://doi.org/10.1190/segam2017-17789671.1

Gu, R.; Hegazy, M.; Zdraveva, O.; 2018. Geologic structure-based image enhancement with directional image partitions, SEG Technical Program Expanded Abstracts, Doi: https://doi.org/10.1190/segam2018-2996337.1

Hale, D.; 2011. Structure-oriented bilateral filtering of seismic images, SEG Technical Program Expanded Abstracts, Doi: https://doi.org/10.3997/2214-4609.201400384

Moore, I.; Kostov, C.; 2002. Stable, efficient, high-resolution Radon transforms, EAGE Expanded Abstracts, Doi: https://doi.org/10.3997/2214-4609-pdb.5.F034

Nichols, D.; Ruse, A.; Hydal, S; 2017. Separating diffractions and specular reflections after imaging, 79th Annual International Conference and Exhibition, EAGE, Extended Abstracts, Doi: https://doi.org/10.3997/2214-4609.201700866

Ortin, M.; Ysaccis, R.; Li, H.; Barros, P.; 2020. Combining wave paths to improve Brazil's pre-salt image, Central Santos Basin multi-azimuth reimaging, SEG Technical Program Expanded Abstracts: 3714-3718. Doi: https://doi.org/10.1190/segam2020-3427597.1

Rickett, J.; 2014. Successes and challenges in 3D interpolation and deghosting of single-component marine-streamer data, SEG Technical Program Expanded Abstract, Doi: https://doi.org/10.1190/segam2014-1159.1

Schonewille, M.; Yan, Z.; Bayly, M.; Bisley, R.; 2013. Matching pursuit Fourier interpolation using priors derived from a second data set, SEG Technical Program Expanded Abstracts:. Doi: https://doi.org/10.1190/segam2013-0956.1

Vigh, D.; Starr, E.W.; 2008. 3D prestack plane-wave, full-waveform inversion. Geophysics, Vol. 73, https://doi.org/10.1190/1.2952623

Woodward, M., D. Nichols, O. Zdraveva, P. Whitefield, Johns, T.; 2008. A decade of tomography, Geophysics, Vol. 73, https://doi.org/10.1190/1.2969907

Yu, M.; Yan, Z.; 2011. Flexible surface multiple attenuation using the curvelet transform, SEG Technical Program Expanded Abstracts, https://doi.org/10.1190/1.3627922

Zarkhidze, A.; Rickett, J.; Oraghalum, E.; Lansky, C.; Raskopin, A.; Bloor, R.; 2016. Adaptive deghosting for complex geometries in the Gulf of Mexico, SEG Technical Program Expanded Abstract: https://doi.org/10.1190/segam2016-13868686.1

Zhao, C.; Zdraveva, O.; Gonzalez, A.; King, R.; Gu R.; Chen, S.; 2015. Improving interpretability of subsalt images by image conditioning and enhancement with RTM vector image partitions, 77th EAGE Conference and Exhibition, https://doi.org/10.3997/2214-4609.201412957